Yuile, Adam; Schulz, Alexander; Wiss, Erik; Müller, Jens; Wiese, Steffen

The simulated effect of adding solder layers on reactive multilayer films used for joining processes

Original published in: Applied Sciences. - Basel : MDPI. - 12 (2022), 5, art. 2397, 17 pp.
Original published: 2022-02-25
ISSN: 2076-3417
DOI: 10.3390/app12052397
[*Visited:* 2022-05-16]

applied sciences

MDPI

Article

The Simulated Effect of Adding Solder Layers on Reactive Multilayer Films Used for Joining Processes

Adam Yuile [1,*], Alexander Schulz [2], Erik Wiss [1], Jens Müller [2] and Steffen Wiese [1]

[1] Chair of Microintegration and Reliability, Saarland University, 66123 Saarbrucken, Germany; erik.wiss@uni-saarland.de (E.W.); s.wiese@mx.uni-saarland.de (S.W.)
[2] Faculty of Electrical and Computer Engineering, Department of Electronics Technology, TU Ilmenau, 98693 Ilmenau, Germany; Alexander.Schulz@tu-ilmenau.de (A.S.); jens.mueller@tu-ilmenau.de (J.M.)
* Correspondence: adam.yuile@uni-saarland.de; Tel.: +49-681-302-71827

Abstract: In order to introduce new bonding methods in the area of electronic packaging a theoretical analysis was conducted, which should give substantial information about the potential of reactive multilayer systems (rms) to create sufficient local heat for joining processes between silicon chips and ceramic substrates. For this purpose, thermal CFD (computational fluid dynamics) simulations have been carried out to simulate the temperature profile of the bonding zone during and after the reaction of the rms. This thermal analysis considers two different configurations. The first configuration consists of a silicon chip that is bonded to an LTCC-substrate (Low Temperature Co-fired Ceramics) using a bonding layer that contains an rms and a solder preform. The reaction propagation speed of the reactive multilayer was set to a value of 1 m/s, in order to partially melt a solder preform underneath a silicon chip. The second configuration, which consists only of the LTCC-substrate and the rms, was chosen to study the differences between the thermal outputs of the two arrangements. The analysis of the CFD simulations was particularly focused on interpretations of the temperature and liquid fraction contours. The CFD thermal simulation analysis conducted contains a melting/solidification model which can track the molten/solid state of the solder in addition to modelling the influence of latent heat. To provide information for the design of a test-substrate for experimental investigations, the real behaviour of Pt-100 temperature probes on the LTCC-substrate was simulated, in order to monitor an actual bonding in the experiment. All simulations were carried out using the ANSYS Fluent software.

Keywords: CFD; thermal simulation analysis; reactive multilayer systems; joining

Citation: Yuile, A.; Schulz, A.; Wiss, E.; Müller, J.; Wiese, S. The Simulated Effect of Adding Solder Layers on Reactive Multilayer Films Used for Joining Processes. *Appl. Sci.* **2022**, *12*, 2397. https://doi.org/10.3390/app12052397

Academic Editors: David García Fresnadillo, Christoph Pauly and Karsten Woll

Received: 19 November 2021
Accepted: 27 January 2022
Published: 25 February 2022

1. Introduction

Thermal mechanical stresses are one of the most crucial issues in joining processes in microelectronics. These stresses are usually caused by two factors. Factor one is the differences in thermal expansion of the materials to be joined. Factor two is the high process temperatures that are needed for most joining processes. Eliminating one of the two factors helps to significantly reduce the thermal-mechanical stress after bonding. One idea to achieve this goal is the usage of localised heat in the joining zone without a global heating of the entire assembly. There are different approaches for low-temperature localised bonding techniques. One such method of realising this is to use nanoscale reactive multilayer technologies to deploy a heat source on a targeted area. Established reactive multilayer systems consist of an alternating stack of layers of different metals, such as Fe and Ni, which can create a self-propagating exothermal reaction. One targeted area for the application of these reactive multilayers in microelectronics are additive bonding processes in LTCC technology, in order to prevent critical thermal-mechanical stresses in sensitive structures within the LTCC multilayer.

LTCC provides special 3D-structuring abilities, which enables liquid cooling system integration [1], special biomedical sensors [2–4] and fluidic structures [2,5]. Such LTCC

architectures are sensitive to thermo-mechanical stresses. Another strength is its specific dielectric properties, that make LTCC a very beneficial substrate for specific areas, such as high frequency or millimetre wave circuits [6–8] or RF-antennas (radio-frequency antennas) and radars [7,9]. Other applications of LTCC substrates are power LED (light-emitting diode) packaging [10] and fibre optical applications [11].

In addition to this multifaceted functionality, LTCC packages are capable of offering a high reliability [8,12], with respect to superior thermal mechanical integrity, a high level of hermiticity [8,13] and excellent chemical resistance [13–15]. The requirements for such characteristics make the LTCC technology an excellent candidate for automotive applications [9,12]. However, due to high costs, LTCC applications are presently best suited to specific high-performance applications, such as military, space, biomedical and millimetre wave communication [12].

While the deposition of reactive multilayers on silicon substrates is well-established [16], it is somewhat more challenging to achieve deposition on LTCC substrates. The main hindrance is the intrinsic roughness of the LTCC substrate, the roughness of which ranges from 0.4 to 1 µm [17–19]. The reactive multilayer thin films are constructed from well-defined energetic materials that are heterogenous in their structure and contain stored chemical energy [20]. These multilayers have thin layers of reactants which alternate between layers of different metastable solids, each of which have a thickness in the range of 10–300 nm [21]. These alternating layers are typically combined up to a total thicknesses in the range of ~0.1–300 µm [20]. The layers are chosen based on their ability to make a reaction and to release heat, and the most straight-forward method for obtaining such a multilayer system is by using layer-by-layer magnetron-assisted deposition [22], however alternative approaches such as vacuum deposition and more cost-effective mechanical methods can also be used [23].

Should the reactants by sufficiently perturbed, e.g., through heat, then they begin to spontaneously intermix on the atomic level, as per Figure 1, where the reaction propagates from left to right, releasing heat in the process [24], and once the reaction is initiated, the subsequent heat release is sufficient such that the reaction continues to self-propagate [20]. Alternate methods for initiating the reaction include the means of using an electric spark or laser pulse [22], whereafter the reaction can also continue to self-propagate.

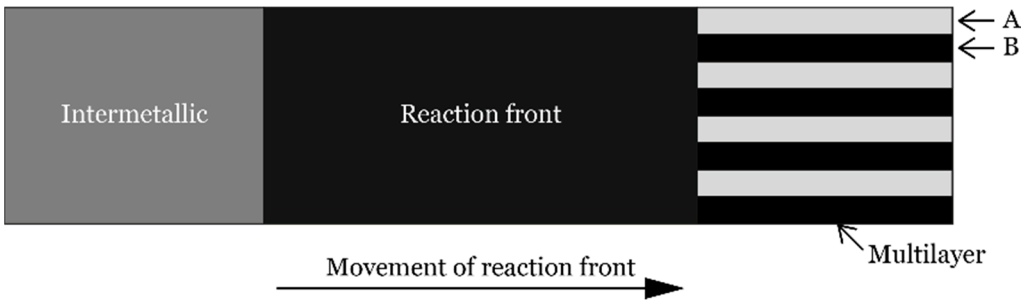

Figure 1. Schematic showing the progression of the reactive multilayer system (RMS).

A successful deposition of reactive multilayers on LTCC substrates has been reported [25]. Here, the LTCC substrates were covered by a brazeable silver system, whereafter an additional 5 µm SAC (Tin–Silver–Copper) solder was deposited to further adapt the rough LTCC substrate to the reactive nanolayer pile.

The intention is to deposit the reactive multilayer on a surface that is well-isolated electrically. In order to adapt the nanolayer pile to the rough surface of the LTCC substrate, a dielectric layer is printed on top, as per Figure 2, with a cross section of the reactive multilayer on an LTCC substrate being shown in Figure 3 complete with a GreenTape™ DuPont (DP) 951 isolation layer. Figure 2 shows the formation required for a so-called tape-on-substrate (TOS) process [26], and furthermore, screen-printed dielectric paste is added to the fired substrate, which then requires a brief drying step and an additional 2 h sintering process.

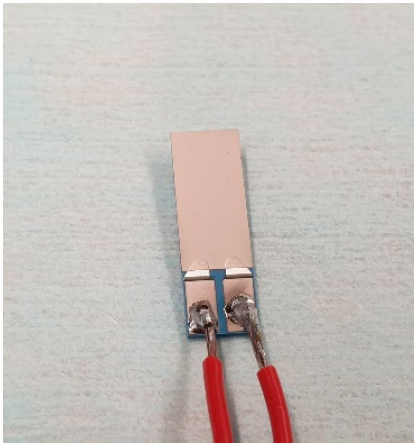

Figure 2. Deposition of dielectric layer on LTCC.

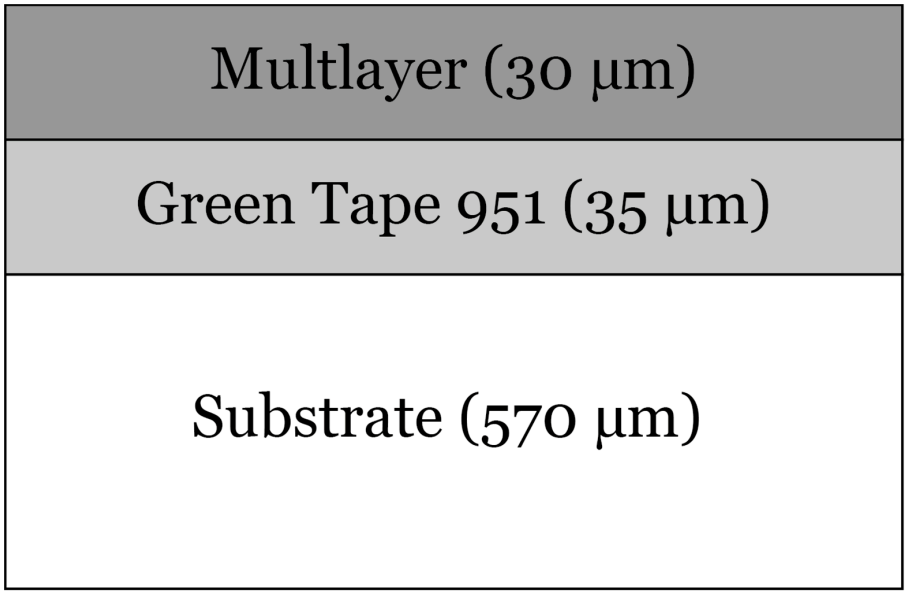

Figure 3. Schematic of reactive multilayer on LTCC substrate with DP 591 isolation layer.

Figure 4 shows a cross-section performed on one of these LTCC substrates with similar embedded temperature probe structures using light microscopy. Here, the reactive multilayer (RMS), the probe and the isolation layer (IL) between the probe and the reactive layer is clearly visible. One can observe from this cross section that each of these structures contains significant roughness, which is not captured in the model where each of the edges are taken to be orthogonal to their respective neighbours and completely straight.

In this work, CFD models are utilised which model and simulate the heat release of such a reactive foil for the purposes of bonding a chip to an LTCC substrate. The localised heat release causes the solder to melt, and thereafter, once the reaction has expired, the structures cool down. The purpose of the simulations is to determine the effect of adding solder layers upon reactive multilayer films and to offer guidelines as to how these would potentially be interpreted by temperature instrumentation in a similar laboratory environment. Comparisons are made between simulations with and without the presence of the solder above the reactive multilayer systems. The CFD models are based on a macroscopic approach and do not take things like surface roughness or pre-treatments to smooth out the layers into account. The simulations are designed towards a generic, hypothetical system as a proof of concept, with the goal of adapting them to experimental configurations for the purpose of comparison when they have been successfully manufactured.

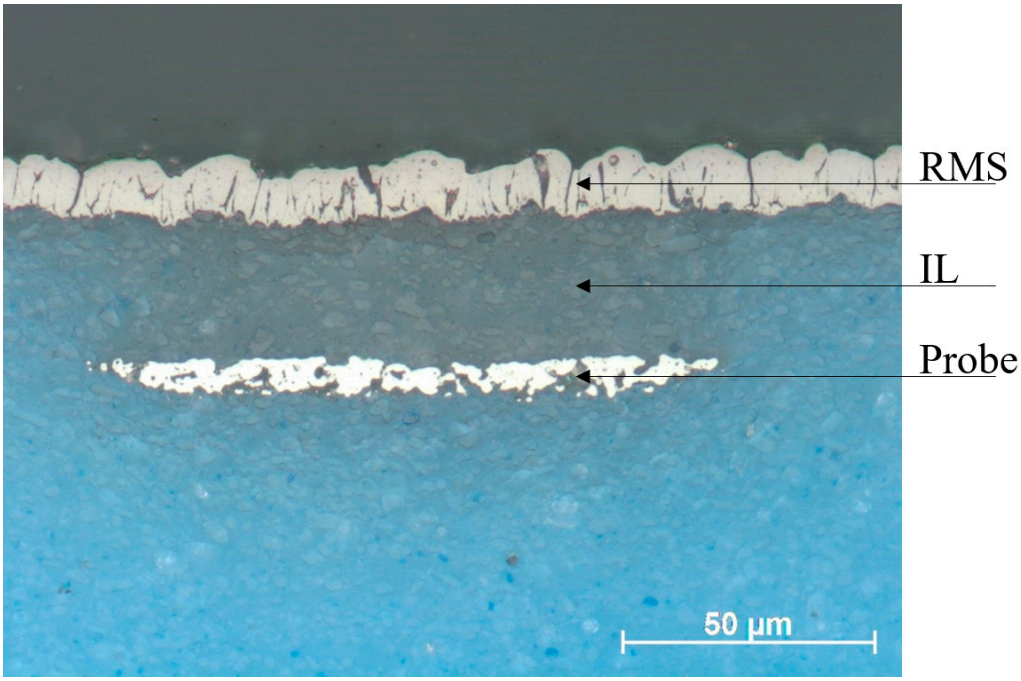

Figure 4. Cross section performed with light microscope.

2. Materials and Methods

There have been various methods used to model reactive multilayer foils that have been studied to enhance the understanding of the limits of their usability and functionality, but these are mainly concentrated on their operating states [27–29] as opposed to their respective performance during manufacture. Therefore, simulations targeting reactive bonding processes in microsystems and microelectronics packaging (such as [30–34]) are generally at an elementary stage compared to the average simulation methodology in the field. The approach used here is the CFD method, as similarly simulated in [35], where a 3-D shoebox model was created comprising various layers, namely a chip, solder, reactive multilayer, substrate and the surrounding air environment.

The extent of the boundaries surrounding the model, where the domain is 20 mm × 20 mm × 15 mm in size, a volume which was chosen to provide sufficient displacement of the external boundaries from the main region of interest whilst maintaining a reasonably sized mesh. The respective thicknesses of the layers were 400 µm for the Si chip, solder thickness of 200 µm, a total reactive foil thickness of 30 µm and an LTCC thickness of 570 µm.

The mesh was subdivided in a manner such that consistent mesh sizing with edge length of 10 µm could be prescribed in the y direction, with a mesh edge length of 100 µm in the x and z directions, as shown in Figure 5. The mesh comprised approximately 5,000,000 cells, representing a mesh significantly larger than that used in similar previous work [35]. The fixed mesh lengths of 100 and 10 µm ensured that the aspect ratio of the cells was within a reasonable range (10:1, for x and z:y), albeit the aspect ratios were slightly larger in the isolation layer, for example, where 4 cells span the 35 µm gap.

Three temperature probes, P1–P3, approximating Pt-100 temperature sensors with silver vias, were integrated into the model inside the LTCC substrate. In Figure 6, the main dimensions of each probe in the x–z plane and the layer thicknesses are shown.

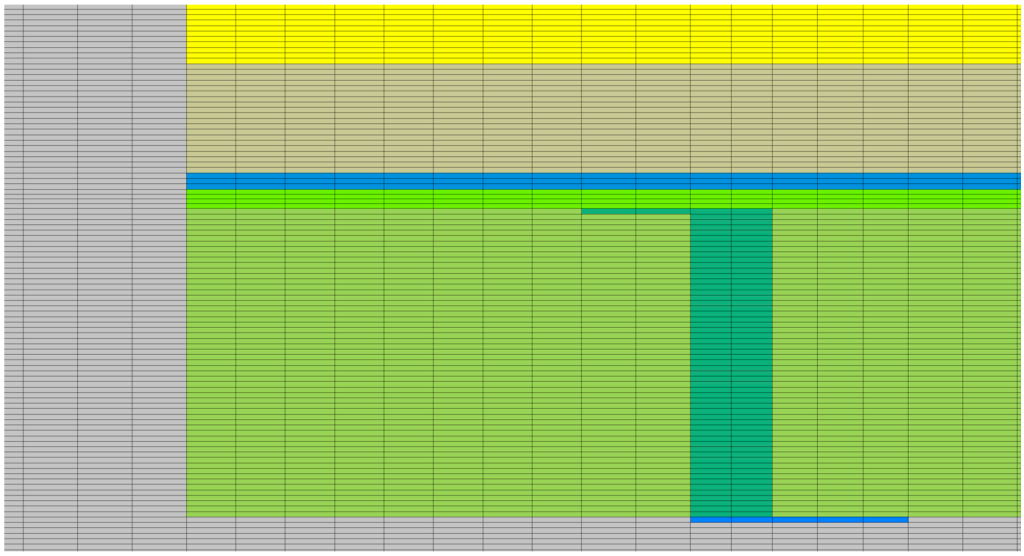

Figure 5. Close-up of mesh of solid structures towards leading edge of reactive foil (Yellow = Si, Brown = Solder, Blue = reactive foil, Green = Green tape ceramics, Turquoise = Temperature probe).

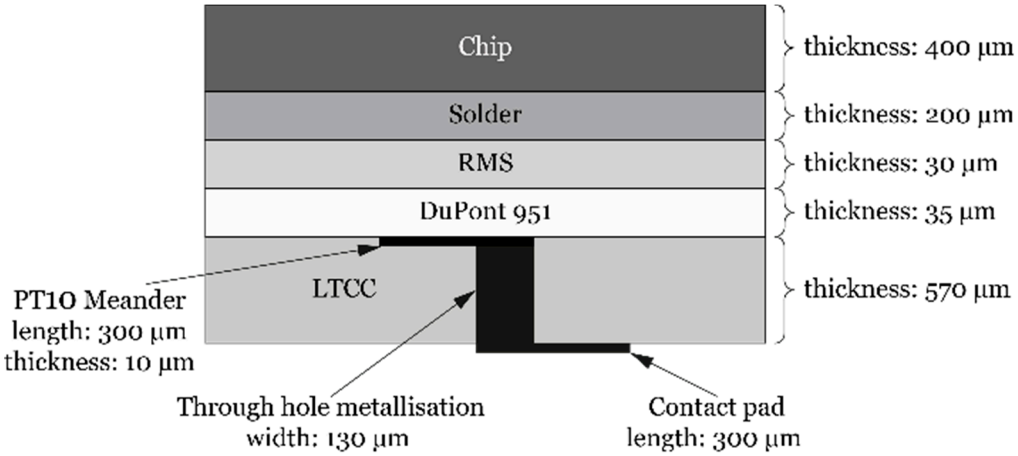

Figure 6. Dimensions of probes and layer thicknesses in x–z plane.

Similarly, in Figure 7, the main dimensions in the x–y plane are illustrated for the model and the 3 temperature probes, P1–P3, are also highlighted.

The sensing volume, i.e., the part for which volume-averaged temperatures were calculated, was 430 µm × 210 µm × 10 µm, corresponding to a sensing volume of 0.0009 mm^3. These probes are displaced from the next probe by 1 mm in the x direction, with the front edge of P1 displaced by 0.3 mm from the leading edge of the reactive multilayer. The top surface is 35 µm displaced below the reactive foil, meaning they are separated by the full thickness of the isolation layer.

Note that there was only one element through the thickness of the Pt probes, which is not ideal, but increasing the number of cells through the thickness of the probes would have a highly detrimental effect on the aspect ratio of the cells, and therefore the stability of the model. These probes were included to help in developing the understanding of the requirements for manufacturing similar prototypes, and furthermore, to understand the interference caused by the presence of the probes themselves.

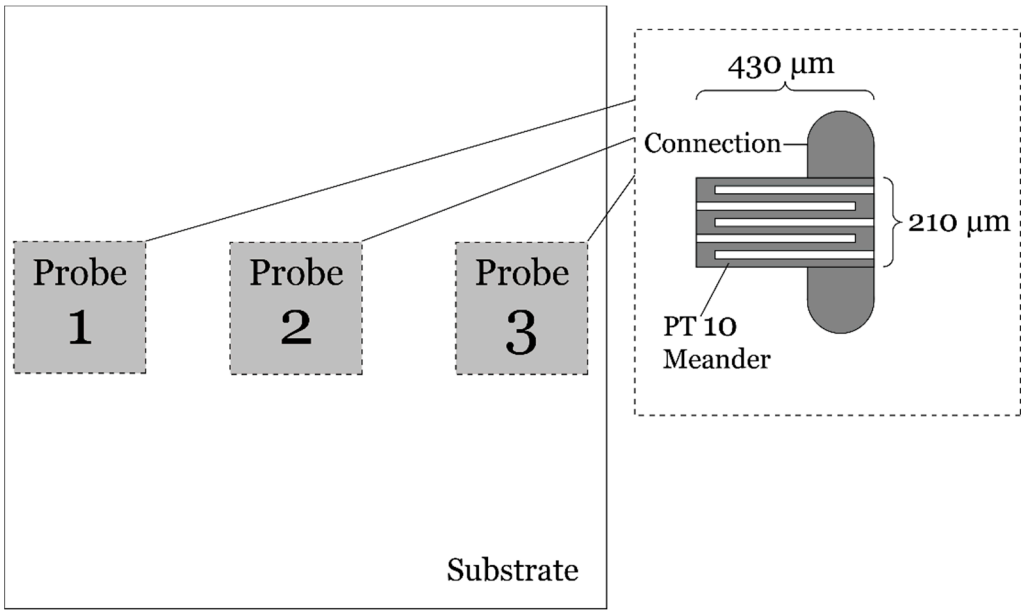

Figure 7. Detailed dimensions in x–y plane.

It is considered to be relatively straight-forward to measure the propagation velocity of reactive foils, due to the intense luminescence of the wave front. However, temperature measurements are more complicated owing to the interference caused by the presence of the thermocouples. The thermocouples are known to typically provide underestimated values of temperature due to their susceptibility to remove heat and interfere with the combustion process [22]. These simulations can offer some insight into the removal of heat, but the heat released will be unaffected by their presence.

The domain comprises both fluid and solid mesh structures, with the respective thermal properties shown in Table 1. These properties are drawn from the ANSYS Fluent material databases and the GreenTape^{TM} DuPont DP 951 material data sheet. The silicon, reactive foil, ceramic, platinum and silver structures have solid states assigned, whereas the air and solder have fluid status and utilise fluid models in the ANSYS Fluent solver. The melting/solidification model is activated in ANSYS Fluent for the solder, in order that the transitions between the molten and solid behaviour, and the associated latent heat transfer throughout, are modelled. The pure solvent melting heat for the solder is 58.5 kJ/kg. A liquidus temperature of 217 °C and solidus temperature of 220 °C were used for the solder. These values correspond closely to typical thermal properties of a SAC solder.

The heat released by the reactive multilayer system was modelled in ANSYS Fluent through a heat source profile in the form of Equation (1). This heat source profile is a probability density function (PDF) propagating in the positive x direction, starting at the leading edge of the reactive multilayer. The reaction is assumed to initiate at time = 0 s and continually propagates as a function of time.

$$Ae^{B(x+C-Dt)^2} \quad (1)$$

The coefficient A corresponds to the amplitude of the reaction wave, 6×10^{12}, B the width of the PDF, -8×10^6, C is an offset to align with the leading edge, 2 mm in the x direction, and D is the velocity of the reaction. For the results presented here, a reaction speed, D, of 1 m/s has been modelled. The reaction speed is known to vary with respect to several factors, for example the ignition potential [21]. In [20], the general range of these multilayer reactions was quoted as being between 0.1 and 100 m/s, therefore a reaction speed of 1 m/s is comfortably within this range. The entire domain was initialised to a temperature of 300 K, in other words no preheating was used.

Table 1. Material properties for solid domains.

	Silicon	LTCC	Solder	Platinum	Silver
ρ kg/m^3	2500	3100	7000	21,460	10,490
Cp J/kg.K	710	600	230	132.04	234.28
K W/m.K	100	3.3	63.2	71.538	419.97

In ANSYS Fluent, the pressure-coupled transient solver is used in combination with the implicitly formulated Volume-of-Fluid (VOF) model complete with 2 Eulerian phases, namely air and solder. The 2-equation k-Ω SST model is used for turbulence modelling with the energy equation also solved numerically. The melting/solidification model, which makes use of the enthalpy–porosity approach [36], was used with a mushy zone parameter of 100,000. This method does not track the melt front explicitly but rather computes a liquid fraction, which indicates the fraction of the cell volume that is in the molten state, i.e., a liquid fraction of 1 corresponds to molten solder, whereas 0 is solder in the solid state.

An inlet boundary condition was specified on the y-max boundary with a velocity of 0.1 m/s, with a corresponding outlet pressure boundary condition at 0 Pa (gauge pressure) on the opposing y min extremity. The turbulence intensity and viscosity ratios were specified to be the same, 0.1% and 10, on each boundary. These boundaries enabled the domain to have incoming and outgoing air, and this was found to be beneficial from a stability standpoint. Given that this crossflow inlet velocity was low, it was considered that artificial crossflow cooling effects would be negligible.

The PISO pressure–velocity coupling method was used with 2nd-order upwind schemes for spatial discretisation. Likewise, for the transient formulation, 2nd-order schemes were used, only this time they were bounded implicit schemes. Furthermore, in order to capture the effects of buoyancy caused by temperature gradients in the air, the Boussinessq approximation was used with a constant thermal expansion coefficient of 0.0034/K.

The time-step size used was 10^{-6} s for 10,000 time steps. Convergence for each conservation equation was achieved for every time step, typically within 100 iterations for the initial time steps, with convergence occurring after just one time step later in the solution process. The temperatures at various probe locations were written out for every time step, with the larger solution files containing field data for the entire domain written out every 100 time steps.

3. Results

The results are presented in two subsections, one for simulations conducted with the presence of a thick layer of solder and a chip above the deposited multilayer on the LTCC, corresponding to Section 3.1, and simulations without the presence of the solder and chip above the reactive multilayer, Section 3.2. These results are first presented individually and then compared more directly in the Section 4.

3.1. Thermal Simulation Results with Solder and Silicon Included

In Figure 8, the temperature contours, for the case with solder and silicon included in the model, are shown 1 ms after the initiation of the reactive foil at the leading edge. The crest of the reaction wave was seen to have propagated approximately 1 mm from the leading edge from time = 0 s, hence corresponding to the prescribed reaction velocity of 1 m/s.

In Figure 9, the temperature contours are shown after 3 ms. The reaction is continuing its propagation from left to right, and approximately half of the silicon has a temperature over 100 °C. The heat release is seen to penetrate relatively well in the positive z-direction, in other words in the direction of the solder from the reactive multilayer, and much less so in

the negative z direction. This is due to the relative disparities in the thermal conductivities and the solder acting as a much better heat sink.

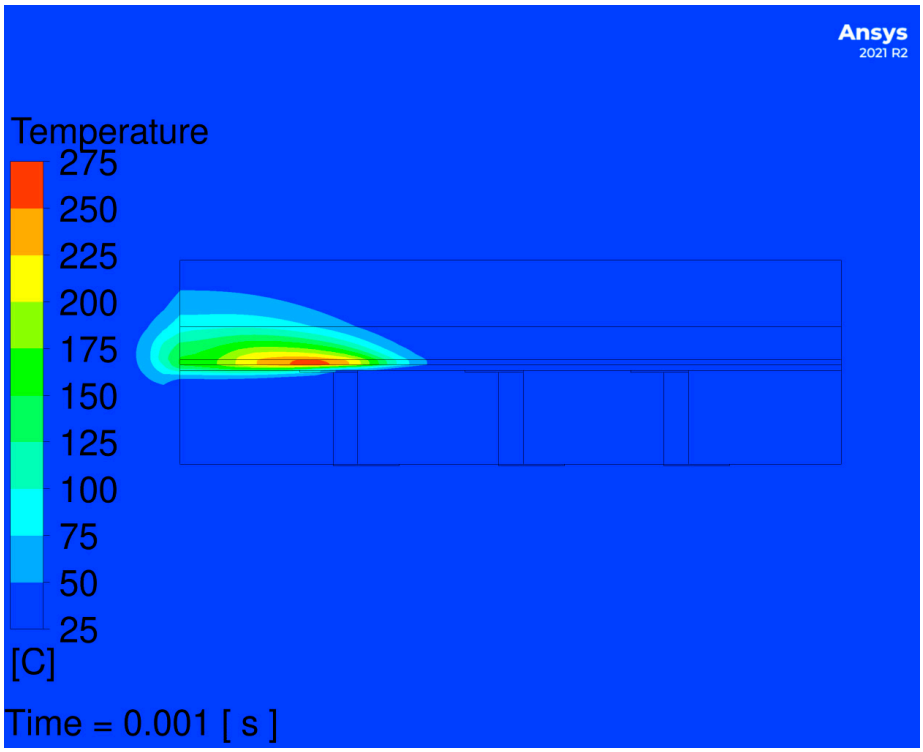

Figure 8. Temperature contours after 1 ms.

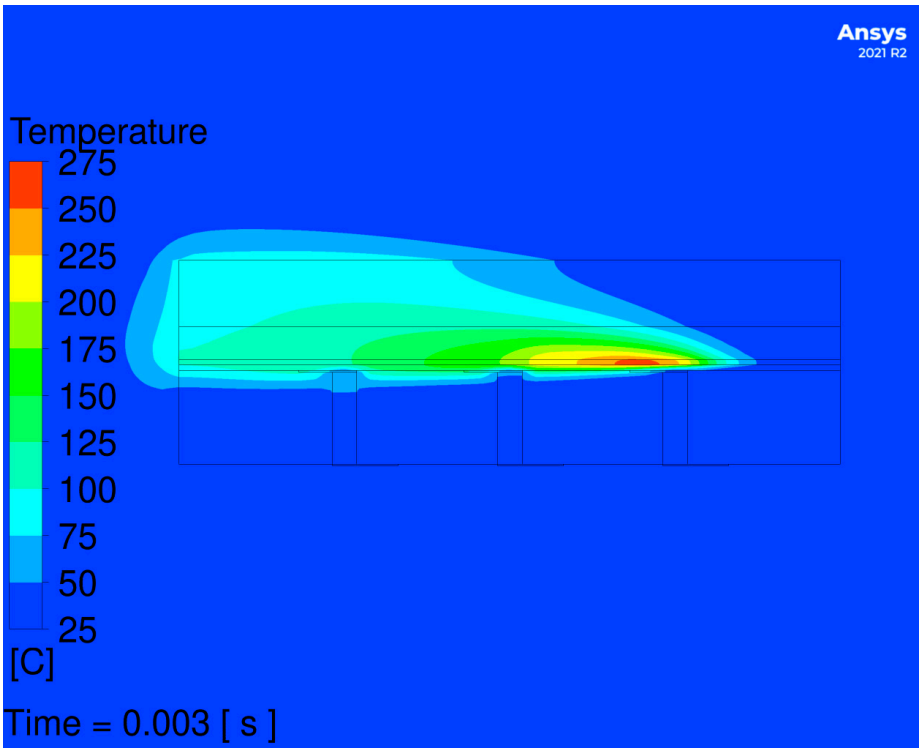

Figure 9. Temperature contours after 3 ms.

Figure 10 shows the liquid fraction contours in the solder region after 3 ms. Here, one can see that there is a small bubble of molten solder adjacent to where, with reference back to Figure 9, the main reaction wave crest is present. Upstream of this bubble of molten solder, one can observe that the solder resolidifies as the wave passes and the structures begin to cool down again. Only a small percentage of the solder is melted in this case as the solder used in this model is very thick.

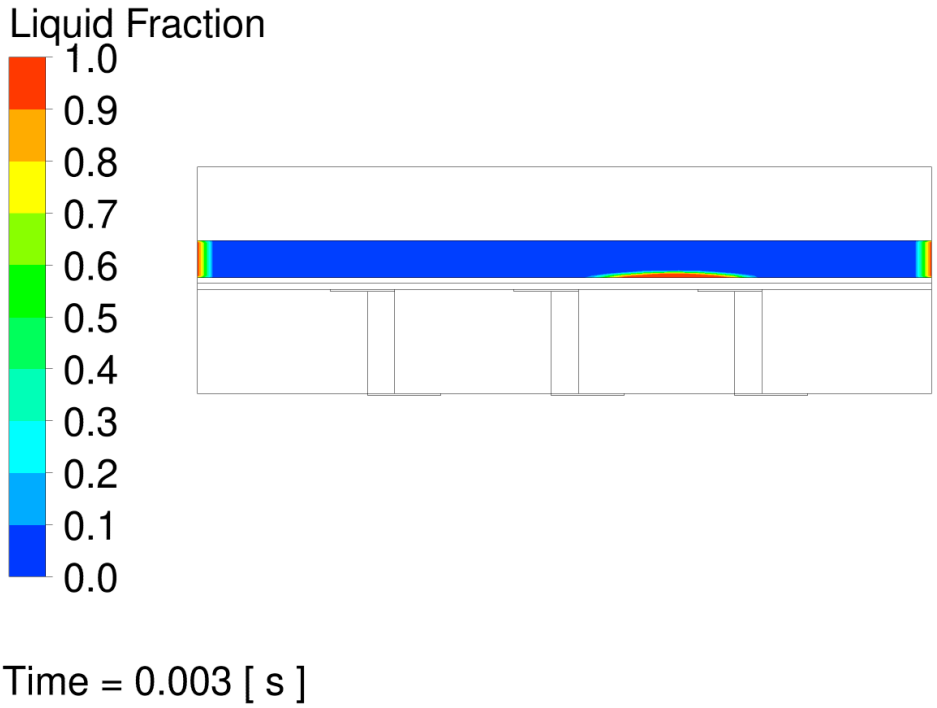

Figure 10. Contours of liquid fraction after 3 ms.

Figure 11 shows the temperature contours at 4 ms, corresponding approximately to the time of reaction exhaustion. By this stage, almost all of the silicon has reached over 100 °C, but the LTCC still has a large percentage of its structure holding on to its initial temperature of 27 °C (300 K).

In Figure 12, the temperature contours are shown 10 ms after reaction initiation, which corresponds to the final time step solved for in the model, time step 10,000. By this point, the reaction wave has long since passed and the backside of the LTCC is still largely unaffected. There is by this point a significant amount of heat which is conducted down through the silver vias, and by this point it is clear that there is some disturbance around the sensing volumes of the probes caused by the presence of these structures. It seems as though the vias act somewhat as a heat sink for the probes, but interpreting results through the thickness of the probes should be exercised with caution here, given that there is only one element through the probe thickness.

In Figure 13 the time–temperature histories of the three probe locations, P1–P3, are shown. Three clear peaks are observed in each of the temperature probes, and by measuring the time offset between these three peaks one would be able to 'sense' the propagation of the reaction at this isolation depth of 35 μm within the LTCC substrate. Based on these simulations, temperature probes manufactured to this specification should be capable of measuring a reaction, at least in the 1 m/s range, assuming that the sampling frequency and frequency response of the temperature measuring equipment was of sufficient specification.

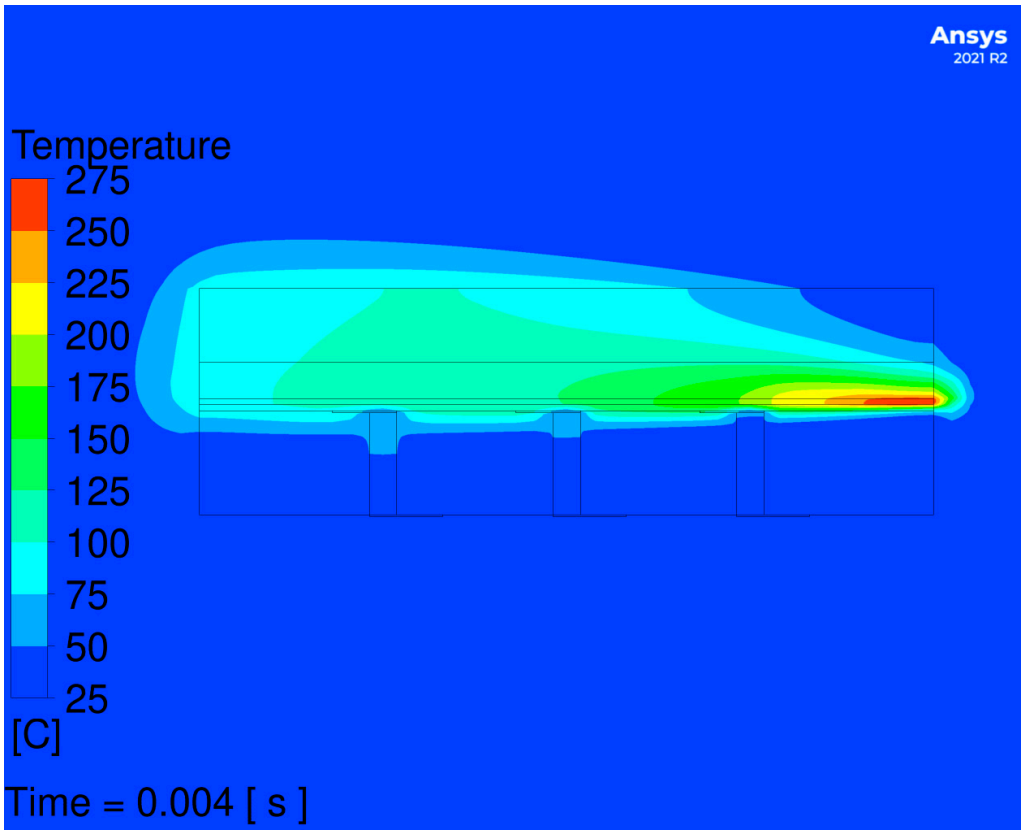

Figure 11. Temperature contours after 4 ms.

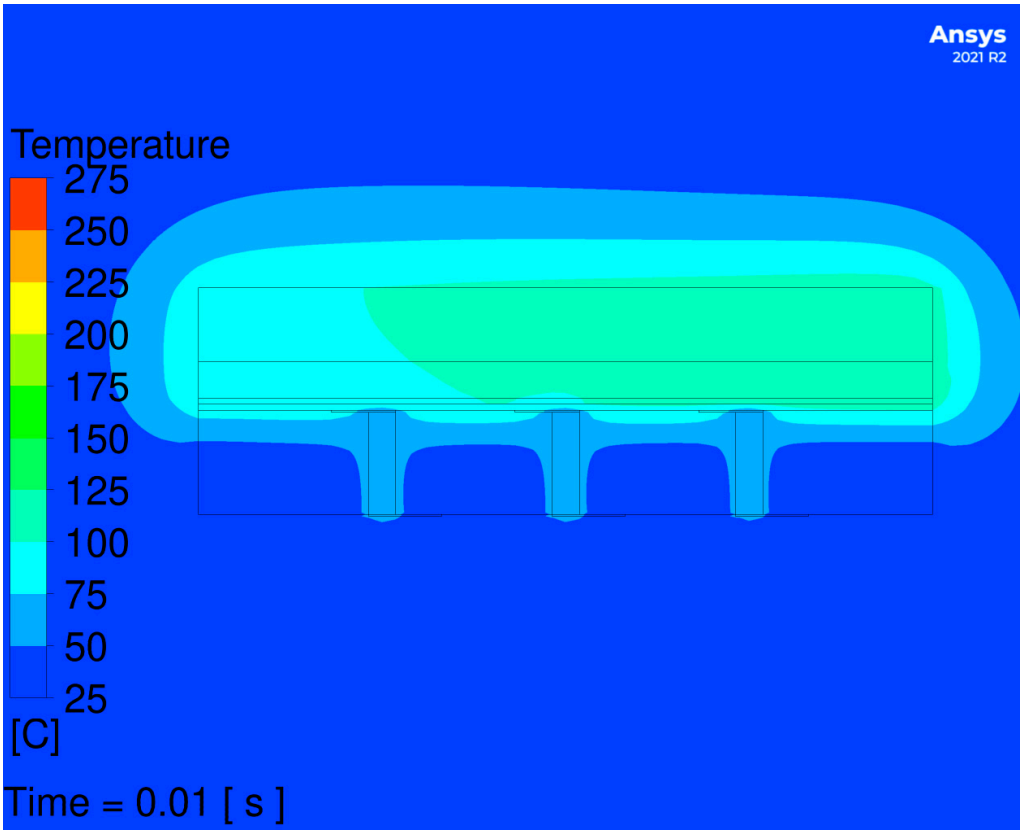

Figure 12. Temperature contours after 10 ms.

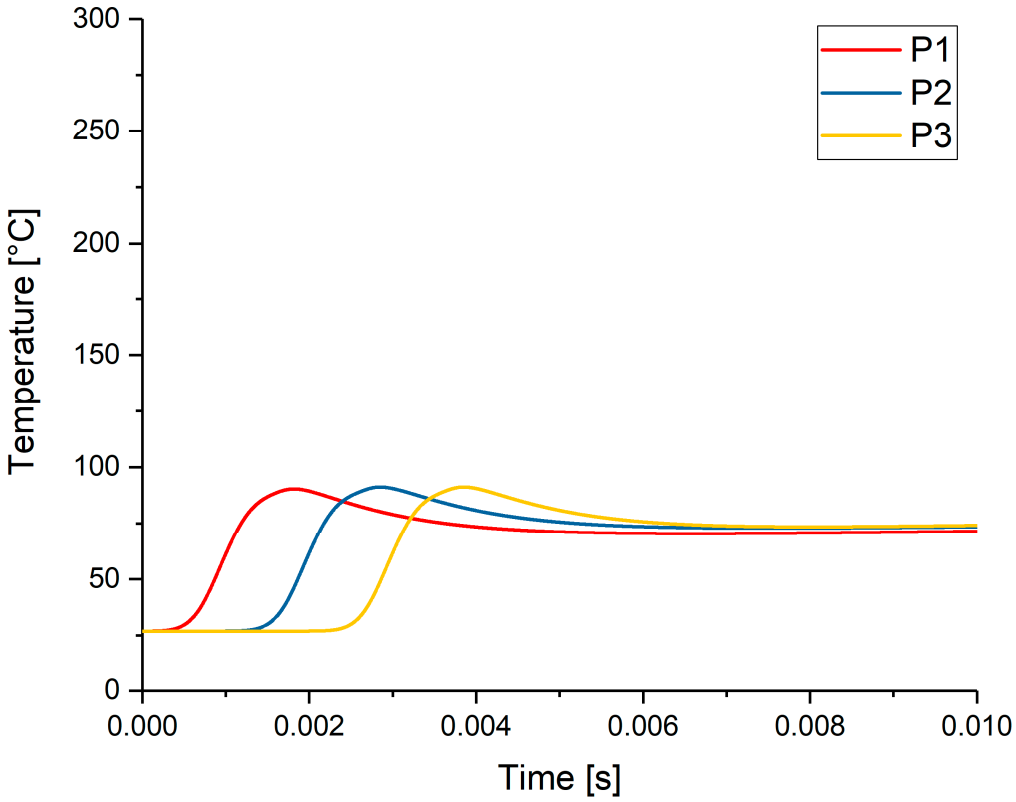

Figure 13. Time–temperature history for the three temperature probes, P1–P3, with solder and silicon included in the model.

3.2. Thermal Simulation Results without Solder and Silicon

Simulations were also performed on an almost identical model as those in Section 3.1, only the solder and silicon were removed and replaced directly with air. No solder was therefore included in these simulations and therefore the melting/solidification model parameters were not required to be solved for numerically.

Figure 14 shows the temperature contours for a reactive foil with the exact same heat release UDF equation as in Section 3.1 after 3 ms. The results are qualitatively very similar to that of Figure 9 but the temperatures are significantly higher, owing to the absence of the solder acting as a heat sink for the exothermic heat release. The peak temperatures for this particular heat-release profile reach a temperature of approximately 800 °C.

Figure 15 again shows the temperature contours post exhaustion, for 10 ms after the initiation of the reaction. Here, again the contours are qualitatively similar to the counterpart including solder and silicon of Figure 12, but the temperatures are quantitatively much higher.

Figure 16 shows the time–temperature history of the three temperature probes embedded in the LTCC, P1–P3. The peaks are similar to those in Figure 13, but the first peak is slightly lower in magnitude than the peaks for the P2 and P3 probes because there is more thermal inertia and less spreading of the heat without the heat sink of the solder.

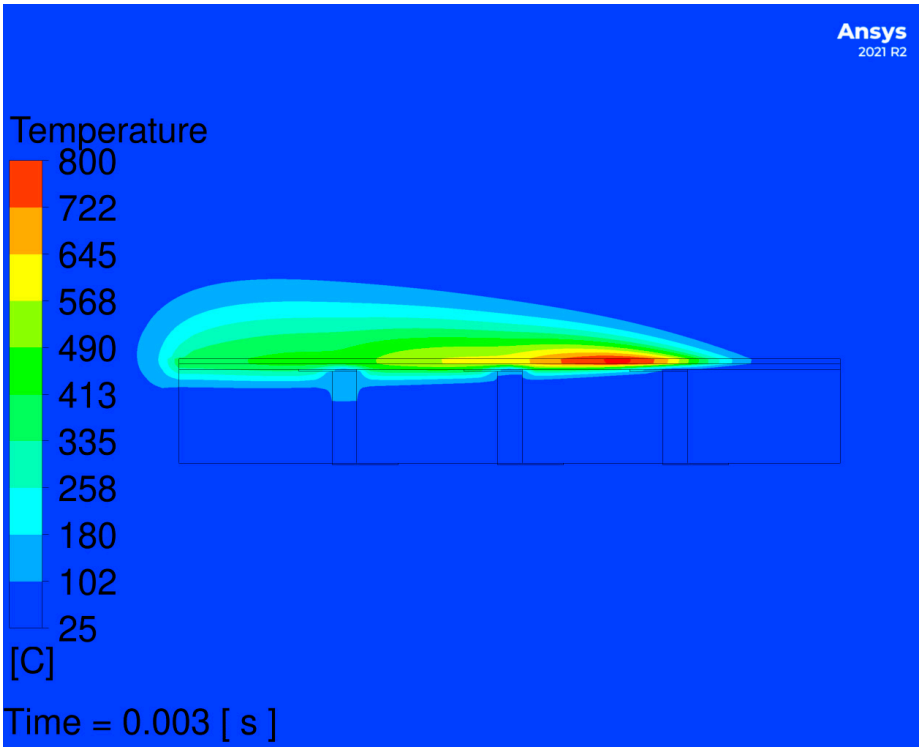

Figure 14. Temperature contours after 3 ms, without solder and silicon.

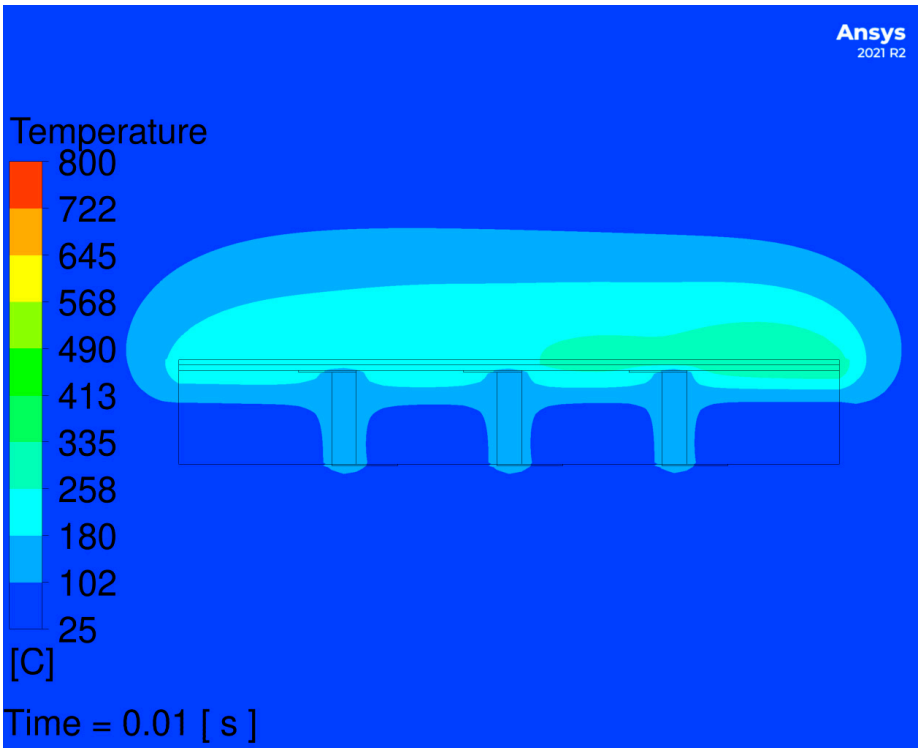

Figure 15. Temperature contours after 10 ms, without solder and silicon.

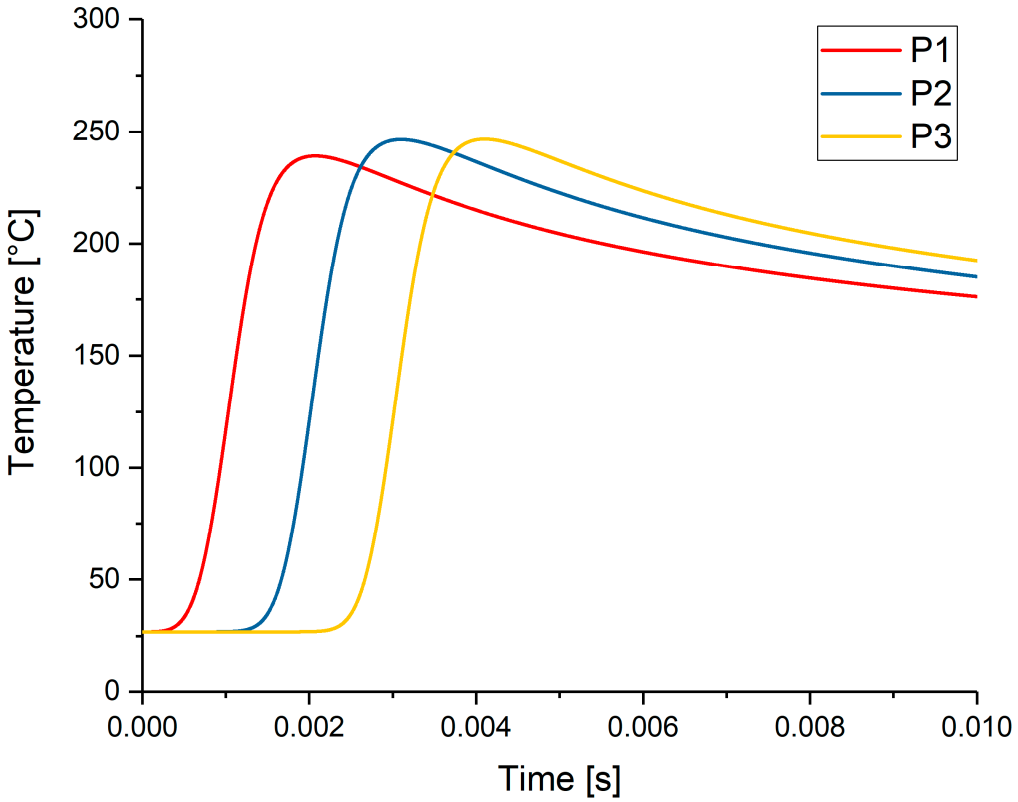

Figure 16. Time–temperature history for the three temperature probes, P1–P3, without solder and silicon.

4. Discussion

In order to make some more detailed comparisons between the two cases discussed, more temperature probes were realised from the models directly above the P2 probes, in the centre of the reactive multilayer system (rms) and the solder, where it exists.

Figure 17 shows the time–temperature progression at each of these locations with the solder and silicon included in the model, whereas Figure 18 shows the time–temperature traces without the solder and silicon. In ANSYS Fluent, vertex-averaged temperatures were used for T_{rms} and T_{solder} and comparing the two figures it is clear that the peak temperatures were much higher without the solder and silicon.

From Figure 17 it is also fair to assume that the heat released from the reactive multilayer propagates far easier in the +z -direction than in the -z direction, in other words, the solder acts to spread the heat much more effectively than the LTCC does.

It is important to note that in a real-world environment the temperature probes would not merely be present in a passive mode but rather they would have current passing through them, resulting in a preheating due to their electrical resistivity, resulting in localised heating, and potentially, further interfering in the reaction process.

In both cases, p_2 is significantly lower than T_{rms}, which is particularly attributable to the presence of the isolation layer between the probe and the reactive multilayer. Nevertheless, probes built to these specifications have been shown to be feasible at this depth.

One thing of particular note in Figure 17 is that during cooldown, kinks in the p_2 and T_{rms} curves are witnessed, due to the latent heat of the solder between the liquidus and solidus temperatures of 220 and 217 °C, but this information is not sensed by the P2 temperature probe. This could be significant in a real-world scenario because the reaction speed may be affected clearly by the presence of the surrounding solder, but also by the effect of the latent heat.

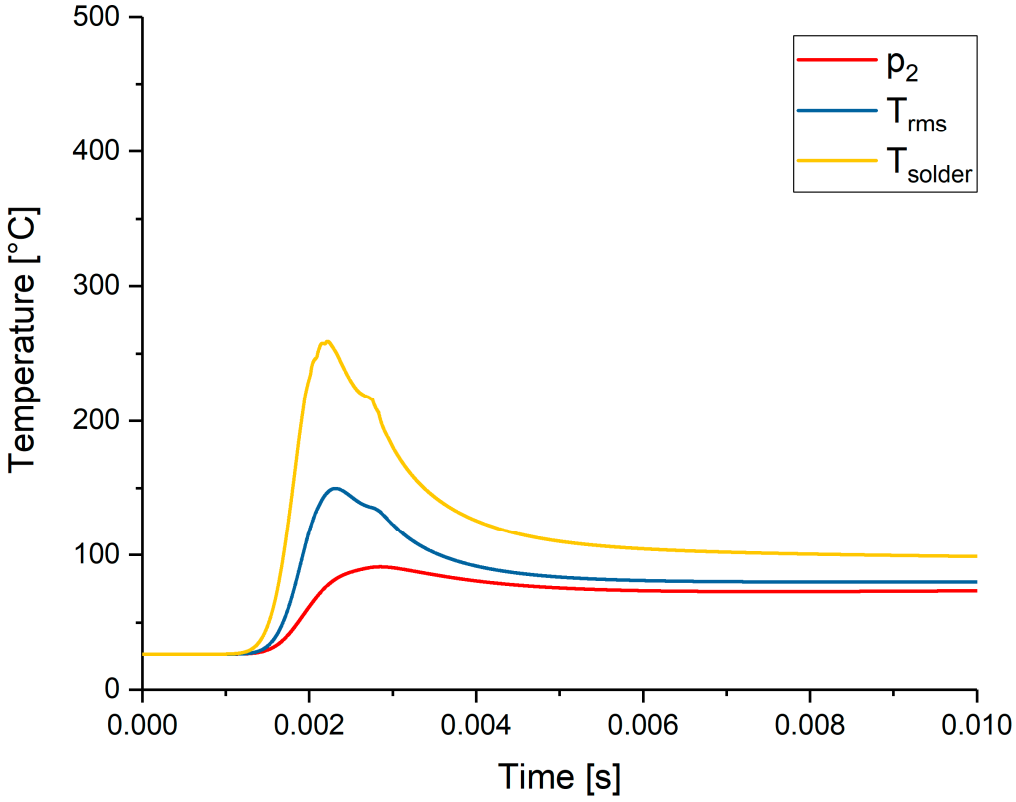

Figure 17. Time–temperature history for three locations, the probe p_2, T_{rms} and T_{solder}.

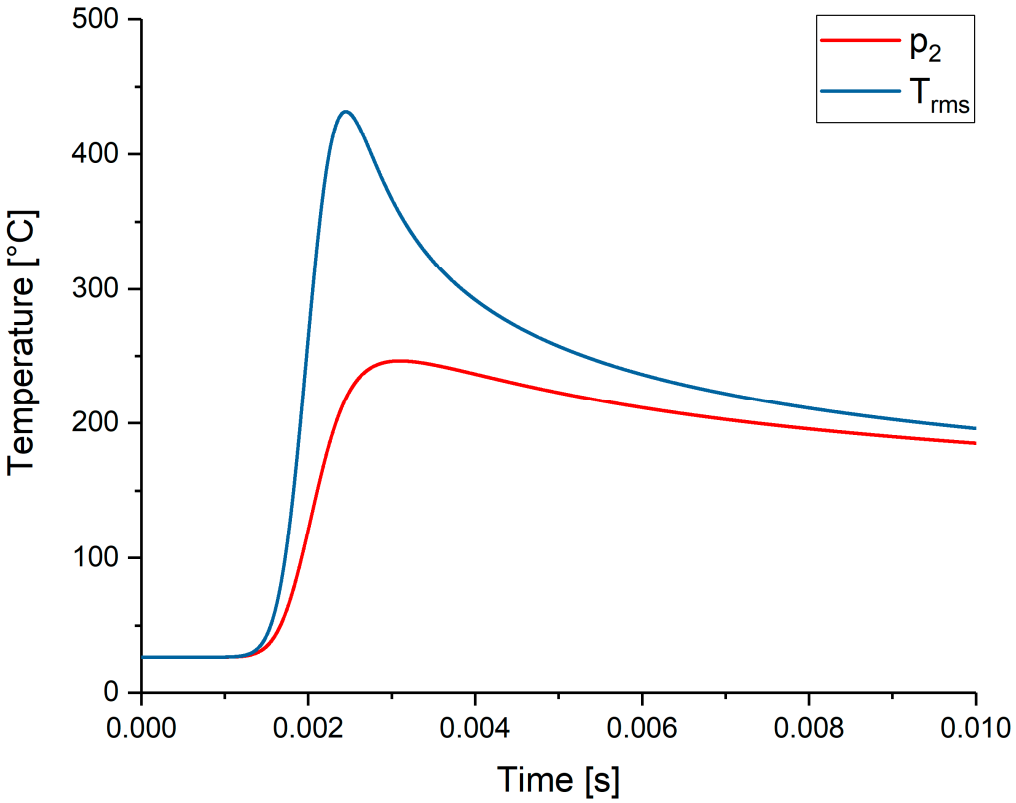

Figure 18. Time–temperature history for p_2 and T_{rms}, without solder and silicon.

5. Conclusions

Thermal CFD simulations have been conducted to simulate the temperature profile of the bonding zone during and after the reaction of the rms. The goal was to estimate theoretically the potential of reactive multilayer systems to create sufficient local heat for joining processes between silicon chips and ceramic substrates. Two different configurations have been considered. The first configuration consists of a silicon chip that is bonded to an LTCC-substrate using a bonding layer that contains a rms and a solder preform, while the second configuration consisted only of the LTCC-substrate and the rms. The simulations are capable of resolving a reaction wave propagating at 1 m/s.

Significant temperature differences were found between the two cases studied here in that the temperatures in the reactive multilayer were much higher for the system without the solder and silicon. The presence of the solder would likely have a significant influence on the real propagation of the reaction through causing greater suppression of the reaction wave. The solder dimensions chosen were extremely thick in order to possess high mesh resolution throughout its thickness and to exaggerate its influence, so the difference between the two configurations may be somewhat exaggerated here.

The enthalpy–porosity method used by the melting/solidification model in ANSYS Fluent allows for incorporation of the effects of latent heat when solving the energy equation, and the encapsulation of this behaviour is something that is not readily available using alternative simulation approaches for an analysis of the solder behaviour during bonding. This means that CFD and these models could offer a leading simulation approach when it comes to assessing the thermal behaviour of reactive foils during bonding. For example, the heat release could potentially be used to determine the total number of layers required to form a functioning solder joint between components. This would effectively offer a crucial insight into manufacturing requirements. Furthermore, a whole new world of multiphysics simulations could be opened by using the temperature fields as inputs to achieve reasonable estimations of stresses induced during a bonding process, and to ultimately determine probable reliability characteristics from these assessments.

Author Contributions: Conceptualization, A.Y., J.M. and S.W.; methodology, A.Y. and A.S.; investigation, A.Y., A.S. and E.W.; supervision, J.M. and S.W.; writing, A.Y.; review and editing, S.W.; funding acquisition, J.M. and S.W. All authors have read and agreed to the published version of the manuscript.

Funding: This research work was supported by funding from the Deutsche Forschungsgemeinschaft (DFG, German Research Foundation)—Project-ID 426204742. The DFG is the German Research Foundation and is a funding institution which promotes science and research in the Federal Republic of Germany.

Acknowledgments: The authors would like to offer particular thanks to Andreas Ruh for his help in preparing cross-sections and for his support in editing the drawings.

Conflicts of Interest: The authors declare no conflict of interest.

References

1. Seok, S.; Kim, J.; Lahti, M. A Study on the Effect of Wire Bonding Interconnects of BCB Capped CPW to CPW on LTCC Substrate. *Microw. Opt. Technol. Lett.* **2014**, *56*, 1378–1381. [CrossRef]
2. Uhlig, P. LTCC Technology for Planar Microwave Antenna Systems. Ph.D. Thesis, Universität Duisburg-Essen and Dresden, Dresden, Germany, 2018.
3. Wilde, J. B4. 1-Trends in Assembly and Packaging of Sensors. *Proc. Sens.* **2009**, *I*, 205–210.
4. Lee, C.K.; Ahn, J.K.; Lee, C.R.; Kim, D.; Baek, B.J. Thermal Analysis of LED Lamp with LTCC-COB Package. *Microelectron. Int.* **2013**, *30*, 3–9.
5. Welker, T. *Methoden Und Technologien Zur Optimierung Der Entwärmung Aktiver Und Passiver Komponenten Auf Keramischen Mehrlagensubstraten*; TU Ilmenau Universitätsbibliothek: Ilmenau, Germany, 2018.
6. Uhlig, P.; Günner, C.; Holzwarth, S.; Kassner, J.; Kulke, R.; Lauer, A.; Rittweger, M. LTCC Short Range Radar Sensor for Automotive Applications at 24 GHz. In Proceedings of the IMAPS 2004—37th Annual Symposium on Microelectronics, Long Beach, CA, USA, 14–18 November 2004; pp. 1–5.

7. Wörhoff, K.; Prak, A.; Postma, F.; Leinse, A.; Wu, K.; Peters, T.J.; Tichem, M.; Amaning-Appiah, B.; Renukappa, V.; Vollrath, G. Photonic Hybrid Assembly through Flexible Waveguides. In Proceedings of the Silicon Photonics and Photonic Integrated Circuits V, International Society for Optics and Photonics, Brussels, Belgium, 3–7 April 2016; Volume 9891, p. 98911P.
8. De Torres, H.B.; Rensch, C.; Fischer, M.; Schober, A.; Hoffmann, M.; Müller, J. Thick Film Flow Sensor for Biological Microsystems. *Sens. Actuators Phys.* **2010**, *160*, 109–115. [CrossRef]
9. Fournier, Y.; Maeder, T.; Boutinard-Rouelle, G.; Barras, A.; Craquelin, N.; Ryser, P. Integrated LTCC Pressure/Flow/Temperature Multisensor for Compressed Air Diagnostics. *Sensors* **2010**, *10*, 11156–11173. [CrossRef] [PubMed]
10. Johannessen, E.; Krushinitskaya, O.; Sokolov, A.; Häfliger, P.; Hoogerwerf, A.; Hinderling, C.; Kautio, K.; Lenkkeri, J.; Strömmer, E.; Kondratyev, V. Toward an Injectable Continuous Osmotic Glucose Sensor. *J. Diabetes Sci. Technol.* **2010**, *4*, 882–892. [CrossRef] [PubMed]
11. Ciosek, P.; Zawadzki, K.; Lopacińska, J.; Skolimowski, M.; Bembnowicz, P.; Golonka, L.J.; Brzózka, Z.; Wróblewski, W. Monitoring of Cell Cultures with LTCC Microelectrode Array. *Anal. Bioanal. Chem.* **2009**, *393*, 2029–2038. [CrossRef]
12. Golonka, L.; Bembnowicz, P.; Jurkow, D.; Malecha, K.; Roguszczak, H.; Tadaszak, R. Low Temperature Co-Fired Ceramics (LTCC) Microsystems. *Opt. Appl.* **2011**, *41*, 383–388.
13. Fournier, Y. *3D Structuration Techniques of LTCC for Microsystems Applications*; EPFL: Lausanne, Switzerland, 2010.
14. Bittner, A.; Schmid, U. The Porosification of Fired LTCC Substrates by Applying a Wet Chemical Etching Procedure. *J. Eur. Ceram. Soc.* **2009**, *29*, 99–104. [CrossRef]
15. Thelemann, T.; Fischer, M.; Groß, A.; Müller, J. LTCC-Based Fluidic Components for Chemical Applications. *J. Microelectron. Electron. Packag.* **2007**, *4*, 167–172. [CrossRef]
16. Adams, D.P. Reactive Multilayers Fabricated by Vapor Deposition: A Critical Review. *Thin Solid Films* **2015**, *576*, 98–128. [CrossRef]
17. Sen, S.; Lake, M.; Kroppen, N.; Farber, P.; Wilden, J.; Schaaf, P. Self-Propagating Exothermic Reaction Analysis in Ti/Al Reactive Films Using Experiments and Computational Fluid Dynamics Simulation. *Appl. Surf. Sci.* **2017**, *396*, 1490–1498. [CrossRef]
18. Rogachev, A.S.; Mukasyan, A.S. Combustion of Heterogeneous Nanostructural Systems. *Combust. Explos. Shock Waves* **2010**, *46*, 243–266. [CrossRef]
19. Rogachev, A.S. Exothermic Reaction Waves in Multilayer Nanofilms. *Russ. Chem. Rev.* **2008**, *77*, 21. [CrossRef]
20. Raić, K.; Rudolf, R.; Ternik, P.; Žunič, Z.; Lazić, V.; Stamenković, D.; Tanasković, T.; Anžel, I. CFD Analysis of Exothermic Reactions in Al-Au Nano Multi-Layered Foils. *Mater. Tehnol.* **2011**, *45*, 335–338.
21. Braeuer, J.; Besser, J.; Wiemer, M.; Gessner, T. A Novel Technique for MEMS Packaging: Reactive Bonding with Integrated Material Systems. *Sens. Actuators Phys.* **2012**, *188*, 212–219. [CrossRef]
22. Bittner, A.; Ababneh, A.; Seidel, H.; Schmid, U. Influence of the Crystal Orientation on the Electrical Properties of AlN Thin Films on LTCC Substrates. *Appl. Surf. Sci.* **2010**, *257*, 1088–1091. [CrossRef]
23. Jantunen, H.; Kangasvieri, T.; Vähäkangas, J.; Leppävuori, S. Design Aspects of Microwave Components with LTCC Technique. *J. Eur. Ceram. Soc.* **2003**, *23*, 2541–2548. [CrossRef]
24. Matters-Kammerer, M.; Mackens, U.; Reimann, K.; Pietig, R.; Hennings, D.; Schreinemacher, B.; Mauczok, R.; Gruhlke, S.; Martiny, C. Material Properties and RF Applications of High k and Ferrite LTCC Ceramics. *Microelectron. Reliab.* **2006**, *46*, 134–143. [CrossRef]
25. Grieseler, R.; Welker, T.; Müller, J.; Schaaf, P. Bonding of Low Temperature Co-Fired Ceramics to Copper and to Ceramic Blocks by Reactive Aluminum/Nickel Multilayers. *Phys. Status Solidi A* **2012**, *209*, 512–518. [CrossRef]
26. Patterson, F.K.; Gantzhorn, J.E.; Daly, T.P.; Rellick, J.R.; Iwabuchi, M.; Kawasaki, S. Tape on Substrate, a New Systems Approach for Manufacturing Multilayer Hybrid Circuits. In Proceedings of the Japan IEMT Symposium, Sixth IEEE/CHMT International Electronic Manufacturing Technology Symposium, Nara, Japan, 26–28 April 1989; pp. 147–151.
27. Liu, S.; Liu, Y. *Modeling and Simulation for Microelectronic Packaging Assembly: Manufacturing, Reliability and Testing*; John Wiley & Sons: Hoboken, NJ, USA, 2011.
28. Madenci, E.; Guven, I. *The Finite Element Method and Applications in Engineering Using ANSYS®*; Springer: Berlin/Heidelberg, Germany, 2015.
29. Rzepka, S. FEM Für Die Mikroelektronik: Erfordernis, Theorie Und Anwendung Der Finiten Element-Methode Bei Der Belastungs-, Schwachstellen-Und Ausfallanalyse Mikroelektronischer Aufbauten Sven Rzepka. Ph.D. Thesis, Universität Duisburg-Essen and Dresden, Dresden, Germany, 2003.
30. Qiu, X. Reactive Multilayer Foils and Their Applications in Joining. Master's Thesis, Louisiana State University, Baton Rouge, LA, USA, 2007.
31. Subramanian, J.S.; Rodgers, P.; Newson, J.; Rude, T.; He, Z.; Besnoin, E.; Weihs, T.P.; Eveloy, V.; Pecht, M. Room Temperature Soldering of Microelectronic Components for Enhanced Thermal Performance. In Proceedings of the Thermal, Mechanical and Multi-Physics Simulation and Experiments in Micro-Electronics and Micro-Systems, Berlin, Germany, 18–20 April 2005; pp. 681–686.
32. Masser, R.; Braeuer, J.; Gessner, T. Modelling the Reaction Behavior in Reactive Multilayer Systems on Substrates Used for Wafer Bonding. *J. Appl. Phys.* **2014**, *115*, 244311. [CrossRef]
33. Wang, J.; Besnoin, E.; Duckham, A.; Spey, S.J.; Reiss, M.E.; Knio, O.M.; Powers, M.; Whitener, M.; Weihs, T.P. Room-Temperature Soldering with Nanostructured Foils. *Appl. Phys. Lett.* **2003**, *83*, 3987–3989. [CrossRef]

34. Amini-Manesh, N.; Basu, S.; Kumar, R. Modeling of a Reacting Nanofilm on a Composite Substrate. *Energy* **2011**, *36*, 1688–1697. [CrossRef]
35. Yuile, A.; Wiese, S. CFD Simulations of Reactive Multi-Layer Usage in Joining Processes. In Proceedings of the 2020 21st International Conference on Thermal, Mechanical and Multi-Physics Simulation and Experiments in Microelectronics and Microsystems (EuroSimE), Cracow, Poland, 5–8 July 2020; pp. 1–5.
36. Voller, V.R.; Brent, A.D.; Prakash, C. The Modelling of Heat, Mass and Solute Transport in Solidification Systems. *Int. J. Heat Mass Transf.* **1989**, *32*, 1719–1731. [CrossRef]